4632 *Chem. Mater.* **2010,** *22,* 4632–4641
DOI:10.1021/cm101225b

CHEMISTRY OF MATERIALS
Article

Ligand-Tuned Shape Control, Oriented Assembly, and Electrochemical Characterization of Colloidal ZnTe Nanocrystals

Feng Jiang,[†] Yunchao Li,*[,†] Mingfu Ye,[‡] Louzhen Fan,[†] Yuqin Ding,[‡] and Yongfang Li*[,‡]

[†]*Department of Chemistry, Beijing Normal University, Beijing, 100875, P. R. China, and* [‡]*Beijing National Laboratory for Molecular Sciences, CAS Key Laboratory of Organic Solids, Institute of Chemistry, Chinese Academy of Sciences, Beijing 100190, P. R. China*

Received April 30, 2010. Revised Manuscript Received July 2, 2010

A novel ligand tuning strategy for the synthesis and assembly of ZnTe nanocrystals is proposed in this paper: a specific ligand is selected to work with the reaction system to regulate (passivate or activate) the reactivity of zinc precursors, as well as the growth and the assembly of resulting nanocrystals in a coordinate way. By utilization of this strategy, high-quality ZnTe nanodots, branched-nanorods (including nanotetrapods), nanowires and microspheres are obtained. Furthermore, by using ZnTe microspheres as building blocks, ordered two-dimensional (2D) and three-dimensional (3D) arrays and well-defined hollow microspheres are fabricated. The size, morphology, and crystal structure of as-prepared ZnTe nanocrystals are well characterized. The underlying mechanisms for ligand-tuned synthesis and assembly of ZnTe nanocrystals are also intensively discussed. Finally, the shape-dependent optical, structural, and electrochemical properties of those ZnTe nanocrystals are systemically investigated; their band edge positions are studied by cyclic voltammetry.

1. Introduction

Colloidal semiconductor nanocrystals (SNCs) have attracted much attention since 1990s because of their unique size-dependent optical and electronic properties, as well as their promising applications in solar cells,[1] light-emitting diodes,[2] biological labeling,[3] and chemical sensing.[4] Therefore, the synthesis,[5] modification,[6] assembly,[7] and application[1−4] of SNCs have been well developed in the last two decades. However, it should be pointed out that, until now, cadmium-based and lead-based SNCs still play a center role in above-mentioned research and applications, which clearly do not accommodate the health and environment needs of the future. Zinc-based SNCs, especially ZnTe and ZnSe nanocrystals, are the promising materials to fill this gap. ZnTe and ZnSe, both are important semiconductor materials with a direct band gap of 2.26 and 2.7 eV, respectively, showing potential applications in blue-green LEDs, solar cells, and so on.

Compared to the well-investigated ZnSe SNCs,[8] ZnTe SNCs not only have a broader tunable wavelength range

*To whom correspondence should be addressed. E-mail: liyc@bnu.edu.cn (Yunchao Li); liyf@iccas.ac.cn (Yongfang Li).

(1) (a) Huynh, W. U.; Dittmer, J. J.; Alivisatos, A. P. *Science* **2002**, *295*, 2425–2427. (b) Sun, B.; Marx, E.; Greenham, N. C. *Nano Lett.* **2003**, *3*, 961–963. (c) Gur, I.; Fromer, N. A.; Geier, M. L.; Alivisatos, A. P. *Science* **2005**, *310*, 462–464. (d) Zhou, Y.; Li, Y. C.; Zhong, H. Z.; Hou, J. H.; Ding, Y. Q.; Yang, C. H.; Li, Y. F. *Nanotechnology* **2006**, *17*, 4041–4047. (e) Koleilat, G. I.; Levina, L.; Shukla, H.; Myrskog, S. H.; Hinds, S.; Abraham, A. G. P.; Sargent, E. H. *ACS Nano* **2008**, *2*, 833–840.

(2) (a) Coe, S.; Woo, W. K.; Bawendi, M.; Bulovic, V. *Nature* **2002**, *420*, 800–803. (b) Tessler, N.; Medvedev, V.; Kazes, M.; Kan, S.; Banin, U. *Science* **2002**, *295*, 1506–1508. (c) Jang, E. J.; Jun, S.; Pu, L. S. *Chem. Commun.* **2003**, 2964–2965. (d) Sun, Q. J.; Wang, Y. A.; Li, L. S.; Wang, D. Y.; Zhu, T.; Xu, J.; Yang, C. H.; Li, Y. F. *Nat. Photonics* **2007**, *1*, 717–722.

(3) (a) Bruchez, M.; Moronne, M.; Gin, P.; Weiss, S.; Alivisatos, A. P. *Science* **1998**, *281*, 2013–2016. (b) Chan, W. C.; Nie, S. M. *Science* **1998**, *281*, 2016–2018. (c) Han, M. Y.; Gao, X. H.; Su, J. Z.; Nie, S. M. *Nat. Biotechnol.* **2001**, *19*, 631–635. (d) Michalet, X.; Pinaud, F. F.; Bentolila, L. A.; Tsay, J. M.; Doose, S.; Li, J. J.; Sundaresan, G.; Wu, A. M.; Gambhir, S. S.; Weiss, S. *Science* **2005**, *307*, 538–544.

(4) (a) Sberveglieri, G.; Depero, L. E.; Ferroni, M.; Guidi, V.; Martinelli, G.; Nelli, P.; Perego, C.; Sangaletti, L. *Adv. Mater.* **1996**, *8*, 334–337. (b) Law, M.; Kind, H.; Kim, F.; Messer, B.; Yang, P. D. *Angew.Chem,. Int. Ed* . **2002**, *41*, 2405–2408. (c) Nazzal, A. Y.; Qu, L.; Peng, X. G.; Xiao, M. *Nano Lett.* **2003**, *3*, 819–822. (d) Comini, E. *Anal. Chim. Acta* **2006**, *568*, 28–40.

(5) (a) Murray, C. B.; Norris, D. J.; Bawendi, M. G. *J. Am. Chem. Soc.* **1993**, *115*, 8706–8715. (b) Qu, L.; Peng, Z. A.; Peng, X. G. *Nano Lett.* **2001**, *1*, 333–337. (c) Zhong, X. H.; Feng, Y. Y.; Knoll, W.; Han, M. Y. *J. Am. Chem. Soc.* **2003**, *125*, 13559–13563. (d) Wang, X.; Zhuang, J.; Peng, Q.; Li, Y. D. *Nature* **2005**, *437*, 121–124. (e) Cozzoli, P. D.; Pellegrino, T.; Manna, L. *Chem. Soc. Rev.* **2006**, *35*, 1195–1208.

(6) (a) Alivisatos, A. P.; Gu, W. W.; Larabell, C. *Annu. Rev. Biomed. Eng.* **2005**, *7*, 55–76. (b) Erwin, S. C.; Zu, L.; Haftel, M. I.; Efros, A. L.; Kennedy, T. A.; Norris, D. J. *Nature* **2005**, *436*, 91–94. (c) Jorge, P.; Martins, M. A.; Trindade, T.; Santos, J. L.; Farahi, F. *Sensor* **2007**, *7*, 3489–3534. (d) Smith, A. M.; Mohs, A. M.; Nie, S. M. *Nat. Nanotechnol.* **2009**, *4*, 56–63.

(7) (a) Murray, C. B.; Kagan, C. R.; Bawendi, M. G. *Annu. Rev. Mater. Sci.* **2000**, *30*, 545–610. (b) Kim, F.; Kwan, S.; Akana, J.r; Yang, P. D. *J. Am. Chem. Soc.* **2001**, *123*, 4360–4361. (c) Shevchenko, E. V.; Talapin, D. V.; Rogach, A. L.; Kornowski, A.; Haase, M.; Weller, H. *J. Am. Chem. Soc.* **2002**, *124*, 11480–11485. (d) Rabani, E.; Reichman, D. R.; Geissler, P. L.; Brus, L. E. *Nature* **2003**, *426*, 271–274. (e) Cui, Y.; Björk, M. T.; Liddle, J. A.; Sönnichsen, C.; Boussert, B.; Alivisatos, A. P. *Nano Lett.* **2004**, *4*, 1093–1098.

(8) (a) Li, L. S.; Pradhan, N.; Wang, Y. J.; Peng, X. G. *Nano Lett.* **2004**, *4*, 2261–2264. (b) Cozzoli, P. D.; Manna, L.; Curri, M. L.; Kudera, S.; Giannini, C.; Striccoli, M.; Agostiano, A. *Chem. Mater.* **2005**, *17*, 1296–1306. (c) Pradhan, N.; Peng, X. G. *J. Am. Chem. Soc.* **2007**, *129*, 3339–3347. (d) Pradhan, N.; Battaglia, D. M.; Liu, Y. C.; Peng, X. G. *Nano Lett.* **2007**, *7*, 312–317. (e) Reiss, P. *New J. Chem.* **2007**, *31*, 1843–1852. (f) Hines, M. A.; Guyot-Sionnest, P. *J. Phys. Chem. B.* **1998**, *102*, 3655–3657.

 Published on Web 07/20/2010

for absorption and emission, but also show the advantage in serving as building material to construct complex nanoarchitectures.[9] Unfortunately, to date, it is still a challenge for synthesis of high-quality ZnTe SNCs in the realm of nanomaterials. Only a few papers have reported the successful preparation of ZnTe nanodots,[9a,b,e,10] nanorods,[10,11] nanowires,[9c,12] and nanoflowers.[10a] However, much work needs to be done in terms of improving overall control in size, shape, and size/shape distribution of ZnTe nanocrystals. In fact, the major issue in preparing ZnTe SNCs is the lack of suitable zinc precursors for matching very active tellurium precursor (tri-*n*-octylphosphine-tellurium, TOPTe, or tri-*n*-butylphosphine-tellurium, TBPTe). Short-chained diethylzinc ($Zn(Et)_2$) and long-chained zinc oleate ($Zn(Ol)_2$) or zinc stearate ($Zn(St)_2$) are generally adopted zinc precursors for synthesizing colloidal ZnTe SNCs. Ironically, $Zn(Et)_2$ is too active,[8e,9a] while $Zn(Ol)_2$ or $Zn(St)_2$ is too passive.[8a,e] None of them can allow the nucleation step go at a proper rate (either too fast or too low), not to mention the fine control of the size and shape of the resulting nanocrystals. Obviously, to solve the above problems, we need to find an effective solution to tune the growth of the resulting nanocrystals, as well as the reactivity of Zn and Te precursors in a coordinate way. Several groups[13] have demonstrated that the ligands in a synthetic system are not only the ligands for the forming nanocrystals but also the ligand for the precursors. Borrowing this concept, we try to employ a ligand tuning strategy to close the synthetic gap existing in ZnTe SNC system.

Oriented assembly, a general approach to manipulate individual nanocrystals as blocking units to form a long-ranged and high-ordered ensembles,[14] has recently demonstrated to be a promising strategy for the preparation of various complex nanostructures.[15] However, the underlying mechanism for this particular phenomenon has not been fully clarified yet. It clearly needs a further understanding of the role that organic ligand and assembly environment play. Answers to these questions not only help to deeply understand the oriented attachment mechanism but also facilitate the practical application of this kind of particular strategy for the shape control and assembly of different nanocrystals.

The development of SNCs-based hybrid solar cells and light-emitting diode (LED) urgently demands an exact knowledge of the band structure parameters (i.e., the highest occupied molecular orbital (HOMO) and the lowest unoccupied molecular orbital (LUMO) energy levels) of nanocrystals. Cyclic voltammetry (CV), a technique generally employed to estimate the HOMO and LUMO energy levels of an electroactive conjugated polymer,[16] has been recently introduced to acquire the band structure information (such as HOMO and LUMO energy levels, defect states, etc.) of SNCs.[17] However, until now, it is still a technical challenge to obtain well-defined redox signals (especially reduction peak) of nanocrystals by CV, owing to the facts that SNCs are generally unstable and sensitive to measurement environment and condition. Therefore, to build up an optimal measurement condition is of practical importance for carrying out intensive electrochemical characterization of SNCs.

Herein, we present a novel ligand tuning strategy for the synthesis and assembly of nanocrystals, that is, a specific ligand was selected to work with the reaction system to regulate the reactivity of precursors, the growth and the assembly of resulting nanocrystals in a coordinate way. By utilization of this strategy, we could not only delicately tune the size and the morphology (from dot, branched nanorod, to wire, and to solid and hollow microsphere) of ZnTe nanocrystals but also assemble them into more complex architectures (such as abates-like nanowire, 2D, and 3D microsphere arrays). Moreover, band-edge positions of ZnTe nanocrystals with various morphologies were systemically studied by CV. To our knowledge, this is the first report on the preparation of high-quality ZnTe hollow microspheres and the systemic characterization of shape-dependent electrochemical properties of SNCs.

(9) (a) Xie, R. G.; Zhong, X. H.; Basche, T. *Adv. Mater.* **2005**, *17*, 2741–2745. (b) Xie, R. G.; Kolb, U.; Basche, T. *Small.* **2006**, *2*, 1454–1457. (c) Dong, A. G.; Wang, F. D.; Daulton, T. L.; Buhro, W. E. *Nano Lett.* **2007**, *7*, 1308–1313. (d) Fiore, A.; Mastria, R.; Lupo, M. G.; Lanzani, G.; Giannini, C.; Carlino, E.; Morello, G.; Giorgi, M. D.; Li, Y. Q.; Cingolani, R.; Manna, L. *J. Am. Chem. Soc.* **2009**, *131*, 2274–2282. (e) Bang, J.; Park, J.; Lee, J. H.; Won, N.; Nam, J.; Lim, J.; Chang, B. Y.; Lee, H. J.; Chon, B.; Shin, J.; Park, J. B.; Choi, J. H.; Cho, K.; Park, S. M.; Joo, T.; Kim, S. *Chem. Mater.* **2010**, *22*, 233–240.

(10) (a) Lee, S. H.; Kim, Y. J.; Park, J. *Chem. Mater.* **2007**, *19*, 4670–4675. (b) Zhang, J.; Sun, K.; Kumbhar, A.; Fang, J. Y. *J. Phys. Chem. C.* **2008**, *112*, 5454–5458.

(11) Jun, Y. W.; Choi, C. S.; Cheon, J. *Chem. Commun.* **2001**, *1*, 101–102.

(12) (a) Li, L.; Yang, Y. W.; Huang, X. H.; Li, G. H.; Zhang, L. D. *J. Phys. Chem. B* **2005**, *109*, 12394–12398. (b) Yong, K. T.; Sahoo, Y.; Zeng, H.; Swihart, M. T.; Minter, J. R.; Prasad, P. N. *Chem. Mater.* **2007**, *19*, 4108–4110. (c) Park, W. I.; Kim, H. S.; Jang, S. Y.; Park, J.; Bae, S. Y.; Jung, M.; Lee, H.; Kim, J. *J. Mater. Chem.* **2008**, *18*, 875–880. (d) Fanfair, D. D.; Korgel, B. A. *Cryst. Growth Des.* **2008**, *8*, 3246–3252.

(13) (a) Yu, W. W.; Wang, Y. A.; Peng, X. G. *Chem. Mater.* **2003**, *15*, 4300–4308. (b) Li, Y. C.; Li, X. H.; Yang, C. H.; Li, Y. F. *J. Phys. Chem. B* **2004**, *108*, 16002–16011. (c) Jun, Y. W.; Lee, J. H.; Choi, J. S.; Cheon, J. W. *J. Phys. Chem. B* **2005**, *109*, 14795–14806. (d) Cho, J. W.; Kim, H. S.; Kim, Y. J.; Jang, S. Y.; Park, J. *Chem. Mater.* **2008**, *20*, 5600–5609.

(14) (a) Penn, R. L.; Banfield, J. F. *Science* **1998**, *281*, 969–971. (b) Penn, R. L.; Banfield, J. F. *Geochim. Cosmochim. Acta* **1999**, *63*, 1549–1557. (c) Colfen, H.; Antonietti, M. *Angew. Chem., Int. Ed.* **2005**, *44*, 5576–5591. (d) Niederberger, M.; Colfen, H. *Phys. Chem. Chem. Phys.* **2006**, *8*, 3271–3286. (e) Zhang, Q.; Liu, S. J.; Yu, S. H. *J. Mater. Chem.* **2009**, *19*, 191–207.

(15) (a) Tang, Z. Y.; Kotov, N. A.; Giersig, M. *Science* **2002**, *297*, 237–240. (b) Zitoun, D.; Pinna, N.; Frolet, N.; Belin, C. *J. Am. Chem. Soc.* **2005**, *127*, 15034–15035. (c) Cho, K. S.; Talapin, D. V.; Gaschler, W.; Murray, C. B. *J. Am. Chem. Soc.* **2005**, *127*, 7140–7147. (d) Pradhan, N.; Xu, H.; Peng, X. G. *Nano Lett.* **2006**, *6*, 720–724.

(16) (a) Eckhardt, H.; Shacklette, L. W.; Jen, K. Y.; Elsenbaumer, R. L. *J. Chem. Phys.* **1989**, *91*, 1303–1315. (b) Li, Y. F.; Cao, Y.; Gao, J.; Wang, D. L.; Yu, G.; Heeger, A. J. *Synth. Met.* **1999**, *99*, 243–248.

(17) (a) Haram, S. K.; Quinn, B. M.; Bard, A. J. *J. Am. Chem. Soc.* **2001**, *123*, 8860–8861. (b) Kucur, E.; Riegler, J.; Urban, G. A.; Nann, T. *J. Chem. Phys.* **2003**, *119*, 2333–2337. (c) Bae, Y.; Myung, N.; Bard, A. J. *Nano Lett.* **2004**, *4*, 1153–1161. (d) Poznyak, S. K.; Osipovich, N. P.; Shavel, A.; Talapin, D. V.; Gao, M.; Eychmuller, A.; Gaponik, N. *J. Phys. Chem. B* **2005**, *109*, 1094–1100. (e) Li, Y. C.; Zhong, H. Z.; Li, R.; Zhou, Y.; Yang, C. H.; Li, Y. F. *Adv. Funct. Mater.* **2006**, *16*, 1705–1716. (f) Inamdar, S. N.; Ingole, P. P.; Haram, S. K. *Chem. Phys. Chem.* **2008**, *9*, 2574–2579. (g) Kucur, E.; Bucking, W.; Nann, T. *Microchim. Acta* **2008**, *160*, 299–308.

2. Results and Discussion

2.1. Ligand Tuning Strategy for the Synthesis and Assembly of ZnTe Nanocrystals. It has demonstrated that some ligands not only can specifically direct the growth of the resulting nanocrystals but can also selectively tune the reactivity of one specific precursor. Since the major issue in preparing ZnTe SNCs is the generally adopted zinc precursors (such as $Zn(Et)_2$, $(Zn(Ol)_2$ or $Zn(St)_2$) are either too active or too passive, we then can take advantage of a ligand tuning strategy to selectively passivate or activate them and thus allow the nucleation step go at a proper rate (see the left part in Scheme 1). To do so, we can add some TOPO, which has proven to bind with Zn atom very tightly,[8e,f] into a synthetic system containing $Zn(Et)_2$, or introduce some alkylamine (such as oleylamine), which has turned out to facilitate the cleavage of zinc carbonate group,[8a,e] into a system containing $Zn(Ol)_2$ or $Zn(St)_2$. Moreover, ligand tuning strategy also offers an opportunity to delicately regulate the growth and assembly of SNCs (see the right part in Scheme 1). For example, to obtain some nanocrystals with anisotropic morphologies, such as tetrapods, we can reintroduce some monomers into the synthetic system to enhance the driving force of reaction environment after the formation of zincblende "seeds" in nucleation step; to avoid renucleate in solution during the epitaxial growth process, we need to add some ligands to improve the stability of monomers. If weakening of the environmental confinement to the seeds by using a weak ligand, the nanocrystals with an isotropic morphology, such as spherical dot, can be finally obtained. To conduct in situ assembly of nanocrystals, we need to create an environment in which not only a burst of nucleation is enabled but also the shape-directing function of ligand is magnified. For example, to assemble nanoparticles into 3D microspheres, we prefer to choose a weak ligand plus a high-temperature environment, in which high surface energy will drive individual nanoparticles to aggregate as many as possible due to limited ligand protection. On the contrary, to assemble nanoparticles into 1D nanowire, a ligand with strong selective adhesion ability is preferred, which can facilitate the assembly of nanoparticles by introducing the dipolar interaction between particles, as well as the interaction between the ligands.

2.2. TOPO-Passivation-Precursor Route to Synthesize ZnTe Nanodots and Branched Nanorods. As mentioned above, $Zn(Et)_2$ is too active for using as zinc precursor to prepare zinc-based SNCs. This limitation can be overcome by the introduction of TOPO to coordinate with $Zn(Et)_2$ before injecting it into a hot solvent, as we demonstrated herein. To prepare ZnTe nanodots, we chose $Zn(Et)_2$, TOPTe, and oleylamine plus ODE or pure oleylamine as zinc precursor, tellurium precursor, and stock solvent respectively, as usual.[9a,b] To examine the tuning effect of TOPO, we specifically added small amount of TOPO to coordinate with $Zn(Et)_2$ first in some cases (protocol A). As shown in Figures 1 and S1 (in Supporting Information), the absorption spectra and TEM images clearly indicate that the size monodispersity

Scheme 1. Sketch Highlighting the Ligand Tuning Strategy for Shape Control and Assembly of Colloidal ZnTe Nanocrystals

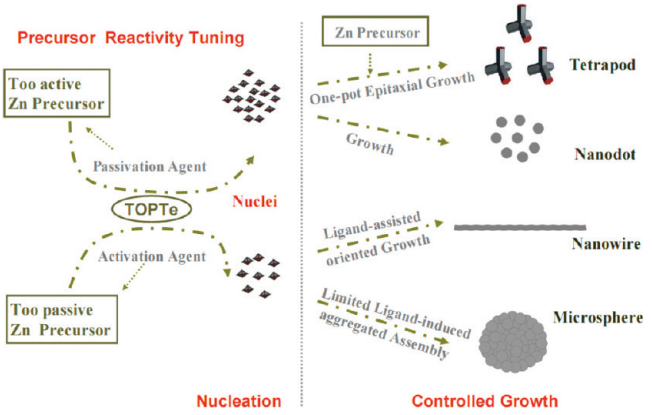

and shape uniformity of ZnTe SNCs become better in the presence of small amount of TOPO in the synthetic system. For example, Figure 1a and b shows the temporal evolution of the absorption spectrum of ZnTe SNCs prepared in oleylamine plus ODE but with or without using TOPO passivation. Compared to the ones prepared in the absence of TOPO (Figure 1b), those ZnTe SNCs synthesized in the presence of TOPO show more definite peaks in their absorption spectra (Figure 1a), which means the size monodispersity is better in the later case. TEM images (Figure 1c and d) reveal that the ZnTe NCs prepared in the above cases all possess a spherical shape and are generally smaller than 5.0 nm. However, the nanoparticles prepared in the presence of TOPO obviously show a better quality in terms of the size and shape distribution (Figure S1, Supporting Information). The insets in Figure 1c and d are their corresponding HRTEM images and SAED patterns. Both confirm that these particles all have zincblende crystal structure, which is consistent with the XRD result shown later in Figure 8b.

Recently, branch-shaped (especially tetrapod-shaped) SNCs have received considerable attention because of their unique optical, electronic, and mechanical properties.[18,19] However, the synthesis of high-quality ZnTe branched nanorods still remains a challenge because of the difficulty in tuning of their nucleation and growth. In order to solve this challenge, we thus designed a ligand-tuning seed-epitaxial growth approach, that is, TOPO-passivated $Zn(Et)_2$ plus TOPTe were added dropwise at a proper rate into the synthetic system to induce the formation of ZnTe branched nanostructures (protocol B). As demonstrated in Figure 2 and Figure S2 (in Supporting Information), epitaxial growth conditions (such as ligand passivation,

(18) (a) Manna, L.; Scher, E. C.; Alivisatos, A. P. *J. Am. Chem. Soc.* **2000**, *122*, 12700–12706. (b) Manna, L.; Millron, D. J.; Meisel, A.; Scher, E. C.; Alivisatos, A. P. *Nat. Mater.* **2003**, *2*, 382–385. (c) Fang, L.; Park, J. Y.; Cui, Y.; Alivisatos, A. P.; Shcrier, J.; Lee, B.; Wang, L. W.; Salmeron, M. *J. Chem. Phys.* **2007**, *127*, 184704−1-184704−6. (d) Talapin, D. T.; Nelson, J. H.; Shevchenko, E. V.; Aloni, S.; Sadtler, B.; Alivisatos, A. P. *Nano Lett.* **2007**, *7*, 2951–2959.

(19) (a) Zhong, H. Z.; Scholes, G. D. *J. Am. Chem. Soc.* **2009**, *131*, 9170–9171. (b) Kim, M. R.; Park, S. Y.; Jang, D. J. *Adv. Funct. Mater.* **2009**, *19*, 3910–3916.

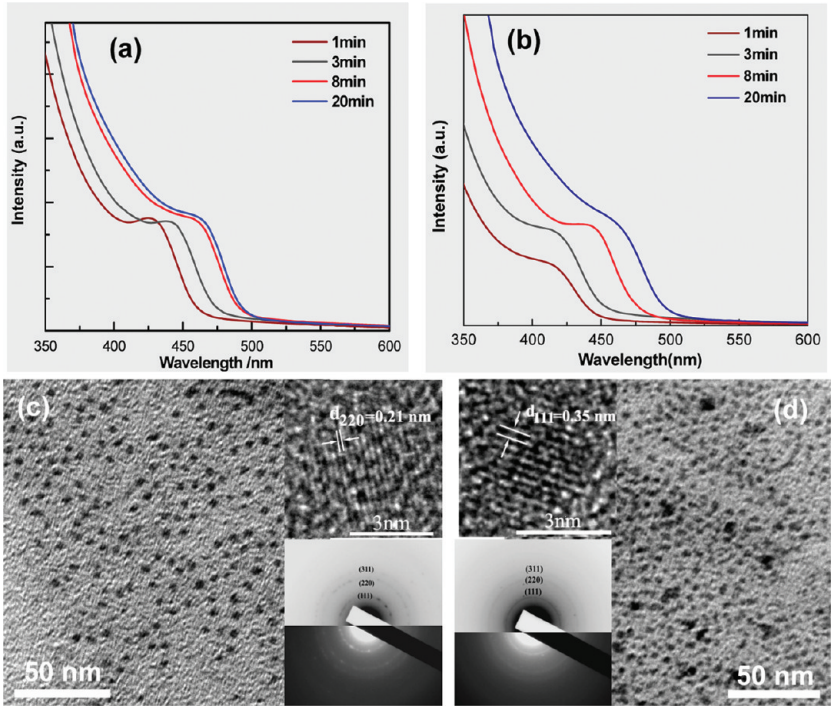

Figure 1. Absorption spectra and TEM images of ZnTe nanodots prepared in the same solvent but using different passivation strategies. (a, b) Temporal evolution of the absorption spectra of ZnTe nanodots prepared in the solution of oleylamine plus ODE but with (a) and without (b) using TOPO passivation of $Zn(Et)_2$. (c, d) TEM images of ZnTe nanodots prepared in above two cases (c corresponds to a and d corresponds to b). The insets in c and d are the corresponding HRTEM images and SAED patterns of such ZnTe nanodots.

reaction temperature, and monomer injection rate) were found to play important roles in determining the final quality of ZnTe branched nanorods prepared according to above protocol. For example, Figure 2a and b are TEM images of ZnTe SNCs prepared in the same solvent but with or without using TOPO passivation. This two images clearly show that the passivation of $Zn(Et)_2$ precursor by adding small amount of TOPO is very helpful to improve the quality of ZnTe branched nanorods. While the images shown in Figure S2 indicate that there exists an optimal reaction temperature for the growth of ZnTe branched nanorods.

However, it should be pointed out the final product is a mixture of two-, three-, and four-armed nanorods. Obviously, the current growth condition needs to be further optimized to obtain high yield of ZnTe tetrapods. In terms of the growth mechanism of these branched nanorods, we believe that the tactful balance of ZnTe SNCs nucleation and growth rate by adopting a proper precursor injection rate and a ligand passivation strategy is the key to form such nanostructures. Such reaction conditions not only enable the formation of zincblende-structured "seeds" in nucleation step but also keep the synthetic system at high reaction potential to drive the growth of multiple arms from the {111} faces of the seeds simultaneously during the following growth step. The crystal structures of the as-prepared ZnTe branched-nanorods (corresponding to Figure 2(a)) were examined by HRTEM and SAED. As shown in Figure 2(c)-2(f) and Figure S3 (Supporting Information), it is quite surprised to find that most arms of the branched-nanorods show zincblende structure but not wurtzite structure as general. A similar phenomenon has been observed previously in the growth of CdTe tetrapods by using TOP instead of TBP as capping ligands.[13d] We think the particular phenomenon observed herein may be attributed to the decrease of monomer reactivity by TOPO passivation, which allows the arms to grow less kinetically and to form a thermodynamically stable phase structure.

2.3. Alkylamine−Activation−Precursor Route to Grow ZnTe Nanowires. Oriented attachment has recently demonstrated to be an effective strategy for the preparation of 1D nanowires or nanorods.[12b,15a,15c,15d] To prepare ZnTe nanowires by using this strategy, we found it is necessary to create a favorable assembly environment, in which nucleation is intentionally accelerated and meanwhile shape-directing function of ligands is magnified. Therefore, stable $Zn(Ol)_2$ was chosen as Zn precursor to stand up high reaction temperature, and ODE plus oleic acid was used as stock solvent to offer a weak coordinate environment; moreover, oleylamine was employed as activating as well as binding agent[8a] and was introduced into the synthetic system together with TOPTe in order to result in a burst of nucleation (protocol C). As shown in Figure 3a−c, the amount of oleylamine that was injected into the synthetic system, exerts an important influence on the final quality of ZnTe nanowires. If no oleylamine was added in, no nanocrystal with regular morphology was produced (Figure 3a). If small amount (0.5 mL) of oleylamine was presented in the system, large-sized nanoparticles accompanying with a low yield of nanowires (average 1 μm long and 20 nm wide) were formed (Figure S4, Supporting Information). With the increase of oleylamine amount in the system, the yield and quality of

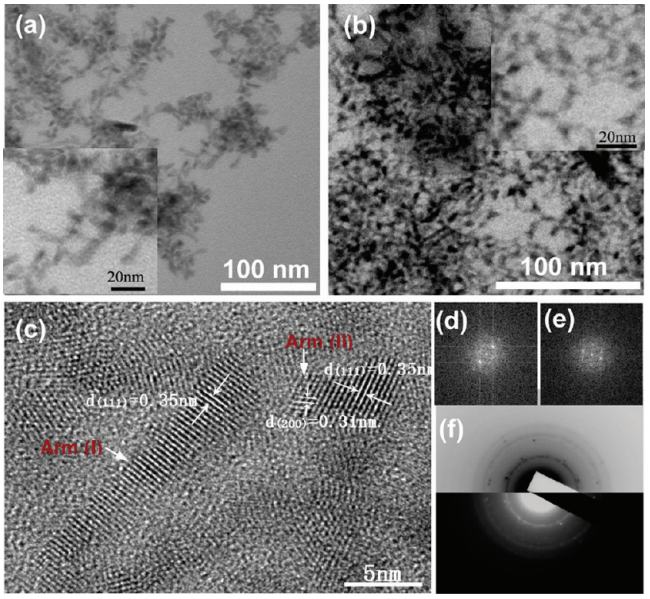

Figure 2. TEM and HRTEM images of ZnTe branched-nanorods prepared in the same solvent but using different passivation strategies. (a, b) TEM images of ZnTe nanorods prepared in ODA with (a) or without (b) using TOPO passivation of $Zn(Et)_2$. (c) HRTEM image and (f) SAED pattern of a. (d, e) FFT-ED patterns corresponding to the arm (I) and arm (II) in c.

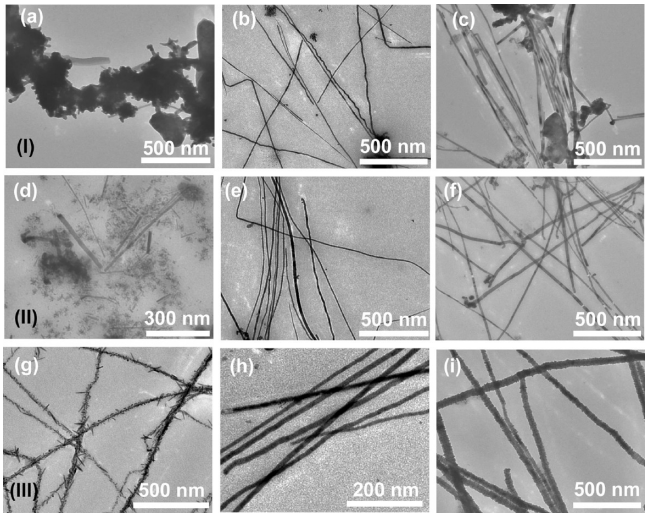

Figure 3. TEM images of ZnTe nanowires prepared by using an alkylamine-assisted activation and assembly strategy and employing different reaction conditions: (I) variation of the injection volume of oleylamine from (a) 0 mL to (b) 1 mL and to (c) 2 mL; (II) variation of the Zn/Te ratio from (d) 4/1 to (e) 2/1 and to (f) 1:4; (III) variation of the ligand passivation mode by adopting (g) insufficient oleylamine passivation, (h) sufficient oleylamine passivation, and (i) TOA passivation.

ZnTe nanowires were improved (average 2 μm long and 12 nm wide) (Figure 3(b)). However, if too many oleylamine existed in the system, the quality of resulting nanowires took a turn for the worse because of the reaction going too violent under such condition. To further clarify the influence of oleylamine, we employed inductively coupled plasma (ICP) atomic emission technique to measure the remaining zinc concentration in synthetic systems at a given moment after oleylamine injection. ICP result (as shown in Figure S5 in Supporting Information) reveals that the remaining zinc concentration in synthetic systems was inversely proportional to the injection amount of oleylamine, indicating that oleylamine does facilitate the cleavage of zinc precursor and thus influences the growth of ZnTe nanowires in above cases. Moreover, as shown in Figure 3d−f, Zn to Te precursor ratio was also found to have a direct effect on the yield and the aspect ratio of ZnTe nanowires. If Zn/Te ratio was set to high, such as 4 in Figure 3d, small branched nanorods was the major product. With the decrease of Zn/Te ratio, the diameter of ZnTe nanowires was increased as well; however, their yield was increased first and then decreased after the ratio down to 1:2 (Figure S4, Supporting Information). It should be pointed out that the optimal Zn/Te ratio for preparation of ZnTe nanowires is around 1. In addition, as shown in Figure 3g−i, the ligand environment was turned out to play an important role in determining the assembly architecture of ZnTe NCs, which is clearly different from the case of CdTe nanowires where ligand molecules were believed to hinder the formation of nanowires.[15a] If oleylamine concentration in the synthetic system was below a threshold value (~0.08 g/mL)), the nanowires with an abates-like morphology were formed (Figure 3g). We believe that incomplete orientation in the assembly process along with insufficient passivation during the annealing process accounts for the formation of such nanoarchitectures. With increasing oleylamine concentration in synthetic system, the nanowires with a smooth surface (Figure 3h) were obtained, which obviously went through a ligand-assisted oriented assembly route (Figure S6 in Supporting Information). If a ligand with large steric effect (such as TOA) was used instead of oleylamine, the nanowires with very rough surfaces were produced (Figure 3i), which is probably attributed to inadequate passivation of their surfaces during the annealing process, though the orientation was done. To support our opinions, XPS technique was used to analyze the surface chemistry of the ZnTe nanowires prepared in above three cases. As shown in Figure S7 in Supporting Information, XPS results confirm that oleic acid was the major ligands for these three types of ZnTe nanowires, and only small amount of oleylamine (or TOA) was bound to their surfaces, especially for the case of abate-like ZnTe nanowires. However, compared to oleic acid and TOA, oleylamine shows a better passivation/etching effect for nanocrystals at high temperature; therefore, only the nanowires formed in the existence of enough oleylamine could get smooth surfaces. Above information indicates that ligand environment dictates the surface passivation of the resulting nanocrystals and further modulates their assemblies and morphologies.

The as-prepared ZnTe nanowires (corresponding to Figure 3e) were also characterized by SEM, EDS, XPS, and HRTEM, respectively. As shown in Figure 4, SEM image confirms these nanowires are quite uniform in terms of their width and length (average 2 μm long and 30 nm wide) as well as high yield in the final product. The difference in the average width of these nanowires revealed by SEM and TEM is mainly due to the adoption of more concentrated solution (including thicker nanowires) for the preparation of SEM specimens. EDS and XPS

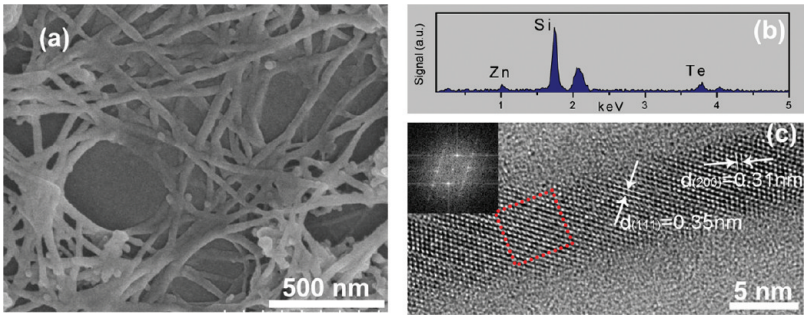

Figure 4. SEM image (a), EDS spectrum (b) and HRTEM image (c) of ZnTe nanowires corresponding to that in Figure 3e. The inset in c is the FFT pattern of the area marked therein.

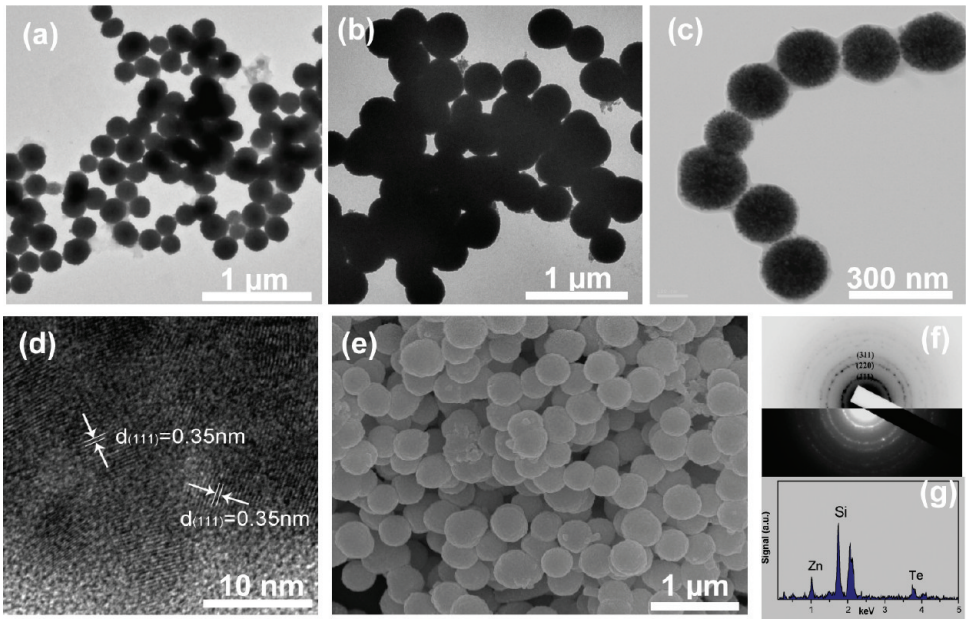

Figure 5. TEM and SEM images of ZnTe microspheres prepared by using a TOA-induced aggregated assembly strategy and employing different precursor concentration: (a) 0.4 and (b) 0.8 mmol $Zn(Ol)_2$. (c) Magnified TEM image and (d) HRTEM image of a; (e) SEM image, (f) SAED pattern, and (g) EDS spectrum of b.

result (Figure 4(c) and Figure S8 in Supporting Information) both reveal the atomic ratio of Zn to Te in these nanowires is ~1:1, which is in good agreement with the stoichiometric ratio in ZnTe, indicating the high-purity nature of them. XPS spectra also confirm the presence of trace amount of Te oxide on their surfaces, signifying these nanowires may partially oxidize when exposed to air. HRTEM image (Figure 4c and Figure S9 in Supporting Information), together with corresponding fast Fourier transform ED (FFT ED), reveals these nanowires are single crystals with a zinc blend structure and gives a interplanar spacing of 0.35 nm for (111) planes and 0.31 nm for (200) planes, respectively.

2.4. Limited Ligand-Induced Synthesis and Assembly of ZnTe Microspheres. Limited ligand protection strategy has recently demonstrated to be an effective and straightforward method for the preparation of nanometer- or micrometer-scaled spherical aggregates.[20] To prepare ZnTe microspheres by utilizing this strategy, we thus chose a relatively weak ligand − TOA as stock solvent to render a limited protection environment, stable $Zn(Ol)_2$ as Zn precursor to accommodate with high reaction temperature (≥280 °C), and TOPTe as Te precursor (protocol D). It was found that monomer concentration, reaction temperature and stirring intensity play a key role in determining the quality and the dimension of ZnTe microspheres. As shown in Figure 5, TEM and SEM images both reveal that the as-prepared ZnTe microspheres are quite uniform and monodisperse (< 10% rms in diameter). Their sizes were found to depend on the monomer concentration in synthetic system and could be tuned from ~200 to 460 nm by variation of $Zn(Ol)_2$ concentration from 0.067 to 0.13 mmol/mL. Closer inspections (Figure 5c and 5d) reveal that the microspheres all have rough surfaces and are composed of many small particles. HRTEM image (Figure 5d) further unveils that those tiny particles are randomly aggregated together and are crystal in nature. Detailed analysis of their lattice fringes gives an interplanar spacing of 0.35 nm, which corresponds well to the distance of 0.35 nm between the

(20) (a) Narayanaswamy, A.; Xu, H. F.; Pradhan, N.; Peng, X. G. *Angew. Chem., Int. Ed.* **2006**, *45*, 5361–5364. (b) Zhong, H. Z.; Wei, Z. X.; Ye, M. F.; Yan, Y.; Zhou, Y.; Ding, Y. Q.; Yang, C. H.; Li, Y. F. *Langmuir* **2007**, *23*, 9008–9013.

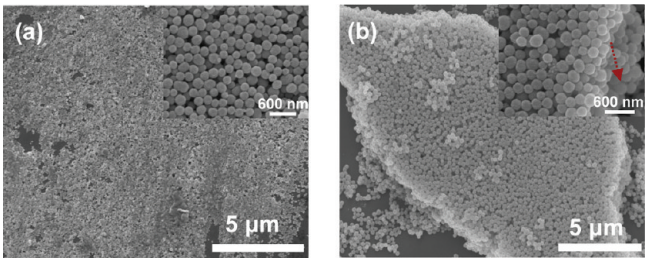

Figure 6. SEM images of 2D arrays (a) and 3D arrays (b) of ZnTe microspheres fabricated on Si substrates by using a slow evaporation and deposition strategy.

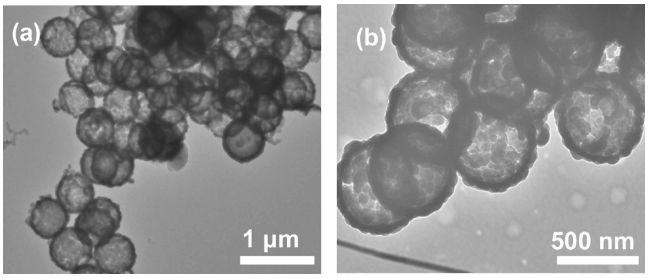

Figure 7. (a) TEM images of ZnTe hollow microspheres prepared by using an ultrasound-assisted conversion of solid microsphere protocol and (b) magnified TEM image of a.

(111) planes of zinc blend ZnTe. The ED pattern (Figure 5d), taking from a randomly chosen microsphere, shows characteristic (111), (220), and (311) diffraction rings, confirming again the polycrystalline nature of the microspheres. EDS result (Figure 5(f)) reveals the atomic ratio of Zn to Te in these microspheres is 1.2: 1, which is in general agreement with the stoichiometric ratio in ZnTe. Moreover, their surface chemistry was examined by FTIR and XPS; as shown in Figure. S10 and Figure S11 in Supporting Information, oleic acid (carboxylate) was found to be the major ligand for those microspheres although they were prepared in pure TOA solvent and carboxylate group only came from zinc oleate. This information indicates that those ZnTe tiny particles and their aggregates (microspheres) were in limited ligand protection environment. To further clarify the formation mechanism of ZnTe microspheres, we intentionally added small amount of oleic acid into TOA solvent. It was surprised to find that only rough nanowires were formed in such situation (see Figure S12 in Supporting Information); which clearly supports the formation of ZnTe microspheres was attributed to the limited ligand protection strategy.

The assembly of monodisperse microspheres into 2D or 3D arrays is of practical importance for the fabrication of photonic band gap crystal and for the investigation of their ensemble properties.[21] To fabricate ordered arrays of ZnTe microspheres on substrates, we took advantage of a slow evaporation and deposition strategy, in which dilute solution of ZnTe microspheres was dropped on precleaned Si sheets and then those sheets were placed in a humid box to allow the microspheres to slowly deposit and aggregate on the substrates during solvent evaporation (protocol G). As shown in Figure 6a and b, large-scaled (in the range of tens micrometer) 2D and 3D arrays of ZnTe microspheres were obtained by utilizing such strategy. In the 2D arrays, the microspheres take a hexagonal closely packing (see the insert in Figure 6a) in the monolayer, however, there still exist some unoccupied and overlapped defects, indicating the assembly condition needs to be further optimized. As for the 3D arrays, closer inspection (the insert in Figure 6b) reveals that they are composed of more than 10 layers of microspheres and the microspheres are generally arranged in a random hexagonal closely packing. It was found that the assembly area and the assembly mode are strongly dependent on the concentration of microspheres in solution, solvent evaporation rate and assembly time.

Monodisperse hollow microspheres have been considered as the ideal functional blocks for application in biomedicine deliveries, sensors and catalyst supports.[22] However, their preparation generally involves complicated heterogeneous-template utilization and removal procedure.[22,23] We present here a simple and straightforward protocol for the preparation of ZnTe hollow microspheres, that is, ultrasound-assisted conversion of solid ZnTe microspheres into their hollow structures (protocol E). As shown in Figure 7a and b and Figure S13 in Supporting Information, upon ultrasound treatment for a few minutes, the ZnTe solid microspheres were converted into well-defined hollow structures. The as-prepared hollow microspheres show a dense (dark) shell and a loose and porous (tint) core. We believe ultrasound treatment facilitating the detachment of tiny particles from the microspheres is the main reason for forming such hollow structures. In addition, the easy formation of hollow structures upon ultrasound treatment indicates that the ZnTe micropheres prepared via a limit ligand protection strategy were not fully compressed.

2.5. Shape-Dependent Optical, Structural, and Electrochemical Properties of ZnTe SNCs. The size- and shape-dependent optical properties are the important character of semiconductor nanocrystals. We systemically compared the absorption and photoluminescence (PL) spectra of as-prepared ZnTe nanodots, branched-nanorods, microspheres and nanowires. As shown in Figure 8a, their absorption edges are located around 500, 518, 540, and 550 nm, respectively. The absorption edges of the nanodots and branched-nanorods are well-defined and blue-shifted in comparison with that of bulk ZnTe (550 nm),

(21) (a) Xia, Y. N.; Gates, B.; Yin, Y. D.; Lu, Y. *Adv. Mater.* **2000**, *12*, 693–713. (b) Gates, B.; Xia, Y. N. *Adv. Mater.* **2000**, *12*, 1329–1332.

(22) (a) Kim, S. W.; Kim, M.; Lee, W. Y.; Hyeon, T. *J. Am. Chem. Soc.* **2002**, *124*, 7642–7643. (b) Chen, G.; Xia, D. G.; Nie, Z. R.; Wang, Z. Y.; Wang, L.; Zhang, L.; Zhang, J. J. *Chem. Mater.* **2007**, *19*, 1840–1844. (c) Cao, S. W.; Zhu, Y. J.; Ma, M. Y.; Li, L.; Zhang, L. *J. Phys. Chem. C* **2008**, *112*, 1851–1856. (d) Wu, Z. C.; Yu, K.; Zhang, S. D.; Xie, Y. *J. Phys. Chem. C* **2008**, *112*, 11307–11313. (e) Zhang, J.; Wang, S. R.; Xu, M. J.; Wang, Y.; Xia, H. J.; Zhang, S. M.; Guo, X. Z.; Wu, S. H. *J. Phys. Chem. C* **2009**, *113*, 1662–1665.

(23) (a) Peng, Q.; Dong, Y. J.; Li, Y. D. *Angew. Chem., Int. Ed.* **2003**, *42*, 3027–3030. (b) Yin, Y. D.; Rioux, R. M.; Erdonmez, C. K.; Hughes, S.; Somorjai, G. A.; Alivisatos, A. P. *Science* **2004**, *304*, 711–714.

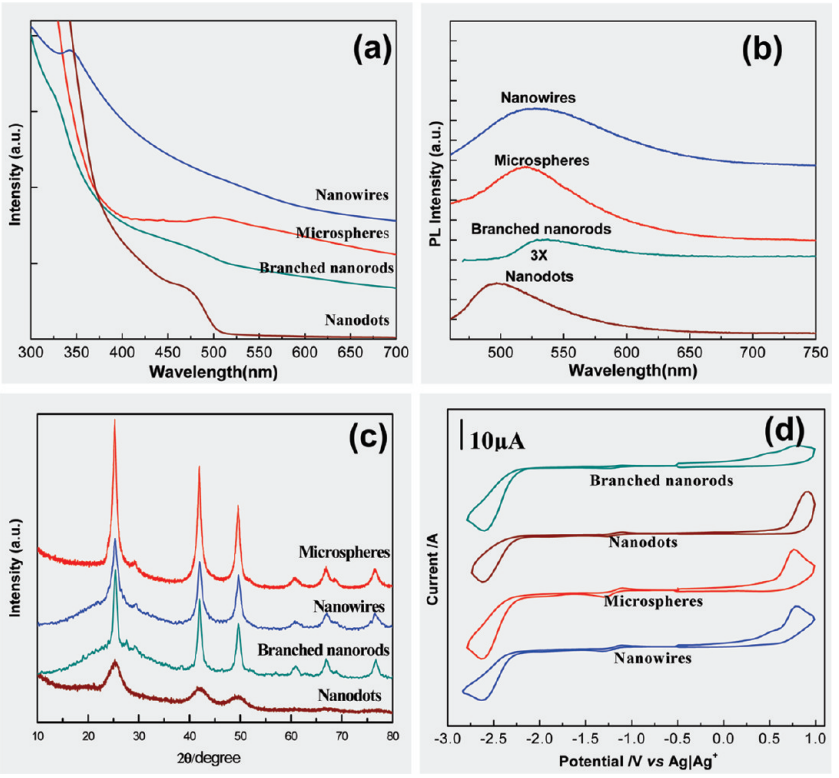

Figure 8. Absorption spectra (a), photoluminescence spectra (b), XRD patterns (c), and cyclic voltammograms (d) of as-prepared ZnTe nanodots, branched-nanorods, microspheres, and nanowires.

indicating both samples have small particle size and narrow size distribution. As for the microspheres, two absorption peaks are shown in its absorption spectrum: the short-wavelength one is sharp and around 510 nm, which corresponds to the bandgap absorption of the tiny particles in the microspheres; the long-wavelength one is broad and locates around 590 nm, which is attributed to the scattering effect from microspheres themselves. While for the nanowires, its absorption edges is quite broad, which is probably due to the large diameter (> 10 nm) of the nanowires, as well as the existence of two direction quantum confinement in this case. In terms of PL property, as demonstrated in Figure 8b, the emission peaks of these four types of ZnTe SNCs are located around 496, 532, 522, and 532 nm, respectively, and are apparently attributed to bandgap emissions. Such a red-shift in emission peaks (from nanodots to nanowires) reflects increasing contribution from the confinement along the long axis of the nanocrystals. Regretfully, we found the PL quantum yield of these ZnTe SNCs were generally low (< 1%), probably because of the inadequate passivation of their surfaces. Therefore, core−shell modification needs to be done in order to improve their PL emission properties.

Figure 8b shows the XRD patterns of the ZnTe nanodots, branched-nanorods, nanowires, and microspheres. These patterns, especially the nanodot one, exhibit broadened diffraction peaks compared to that of bulk ZnTe, signifying the finite size of these crystallites. According to Debye−Scherrer equation, their average sizes in [111] direction are estimated to be 3.4 nm, 6.0 nm, 4.4 and 6.9 nm respectively, which is slightly smaller than the values observed by TEM. All patterns can be definitely indexed as zincblend-phased ZnTe with the strong characteristic (111), (220), and (311) peaks. No peak from other phase is detected in these four patterns. It seems that the morphology of these nanocrystals does not influence their XRD patterns quite much, probably due to the random orientation of them in powder samples.

The HOMO and LUMO energy levels of SNCs can be respectively estimated from the onset oxidation potential (E'_{ox}) and onset reduction potential (E'_{red}) shown in their cyclic voltammograms.[17] To obtain well-defined redox signals, we found it is very important to purify the as-prepared SNCs thoroughly, to carry out the purification and measurement step in a fully inert environment, and to form a SNCs film with an appropriate thickness on electrode surfaces (see Figure S14 in Supporting Information).[17e] By careful optimization of the characterization condition, we obtained well-defined cyclic voltammograms of ZnTe nanodots, branched-nanorods, nanowires and microspheres. As shown in Figure 8(c), the four CV curves all demonstrate a pair of well-separated redox peaks; however, the onset position of redox peaks in these curves are obviously different. Relative to Ag/Ag^+ reference electrode, the onset oxidation and reduction potentials of these nanocrystals are 0.60 and −2.10 V for the nanodots, 0.50 and −2.10 V for the branched-nanorods, 0.40 and −2.15 V for the nanowires, and 0.45 and −2.15 V for the microspheres, respectively. It can be seen that the onset potentials of oxidation and reduction waves are generally negative-shifted with the

Table 1. E_{HOMO}, E_{LUMO}, and E_g values of ZnTe Nanodots, Branched-Nanorods, Nanowires, and Microspheres

	ZnTe nanodots	ZnTe nanotetrapods	ZnTe nanowires	ZnTe microsphere	ZnTe[9e] bulk values
E_{HOMO}/eV	−5.30	−5.20	−5.10	−5.15	−5.0
E_{LUMO}/eV	−2.60	−2.60	−2.55	−2.55	−2.7
E_g/eV (determined by CV)	2.70	2.60	2.55	2.60	2.3
E_g/eV (determined by Abs)	2.50	2.40	2.25[#]	2.30	

increase of "effective" particle size. However, in the case of branched-nanorods and nanowires, there both show an exceptional broad transition region plus a shoulder peak right behind the oxidation peak, which makes the estimation of the onset position difficult. Such situation is believed to be associated with the surface or deep defects existing in these nanocrystals.[17d,g] Table 1 further compares the HOMO energy level (E_{HOMO}), LUMO energy level (E_{LUMO}) and energy bandgap (E_g) values of these nanocrystals determined by CV, and by absorption edge method (only for E_g) with that of bulk ZnTe. It can be seen the E_g values determined by CV are slightly larger than those estimated by absorption edge. The higher electrochemical bandgap than optical bandgap is a common phenomenon for the conjugated polymers,[24] which is probably due to the energy barrier of the charge transfer at the electrodes during the cyclic voltammetry. The E_{HOMO} and E_{LUMO} values of the nanocrystals are found to be generally negative-shifted and positive-shifted respectively in comparison with that of bulk ZnTe,[9e] which is consistent with previous experimental results and theoretical prediction.[17b,25]

3. Conclusions

In summary, we have reported a novel ligand-tuning strategy for the synthesis and assembly of ZnTe nanocrystals. By utilization of this strategy, fine-tuning of the size, morphology, and assembly of ZnTe nanocrystals have been successfully achieved. The thus-prepared ZnTe nanodots, branched-nanorods, nanowires and microshperes are in high quality. Furthermore, by using ZnTe microspheres as building blocks, ordered 2D and 3D arrays of ZnTe microspheres were formed via employing a slow evaporation and deposition strategy, and well-defined hollow microspheres were fabricated through utilizing an ultrasound-assisted conversion method. These results clearly demonstrate that ligand selectivity and reaction environment play a key role in determining the nucleation, growth and assembly of nanoparticles. Moreover, the shape-dependent optical, structural and electrochemical properties of these nanocrystals were systemically investigated. The HOMO and LUMO energy levels of these ZnTe nanocrystals determined by CV were found to be generally negative-shifted and positive-shifted respectively in comparison with that of bulk ZnTe. The band structure information obtained here will be very helpful in fabricating ZnTe-based hybrid devices. Most significantly, we believe that the ligand tuning strategy demonstrated in this paper will throw a new light on how to delicately control the size and morphology as well as the assembly of nanoparticles.

(24) (a) Johansson, T.; Mammo, W.; Svensson, M.; Andersson, M. R.; Ingana, O. *J. Mater. Chem.* **2003**, *13*, 1316–1323. (b) Chen, W. C.; Liu, C. L.; Yen, C. T.; Tsai, F. C.; Tonzola, C. T.; Olson, N.; Jenekhe, S. A. *Macromolecules* **2004**, *37*, 5959–5964. (c) Hou, J. H.; Tan, Z. A.; Yan, Y.; He, Y. J.; Yang, C. H.; Li, Y. F. *J. Am. Chem. Soc.* **2006**, *128*, 4911–4916.

(25) Alivisatos, A. P. *J. Phys. Chem.* **1996**, *100*, 13226–13239.

4. Experimental Section

4.1. Materials. Methanol, ethanol, chloroform, toluene, oleic acid (OA), and zinc oleate ($Zn(Ol)_2$) (Beijing Chemical Reagent Ltd. Co. of China) are analytical grade reagents. Tellurium powder (99.8%, 200 mesh, Alfar), diethylzinc ($Zn(Et)_2$, 15% w/w in hexane, Alfar), 1-octadecene (ODE, tech.90%, Alfar), tri-*n*-octylamine (TOA, 98%, Alfar), trioctylphosphine (TOP, tech.90%, Alfar), trioctylphosphine oxide (TOPO, 98%, Alfar), ferrocene (99%, Alfar), tetra-*n*-butylammonium hexafluorophosphate (98%, Alfar), oleylamine (C18-content 80−90%, Aldrich), and octadecylamine (ODA, 97%, Aldrich) were used as received without further purification. Acetonitrile (Spectrum Pure, Tianjin JinKe Research Institute of Fine Chemicals) was distilled before use.

4.2. Synthesis of ZnTe Nanocrystals. Generally, all ZnTe nanocrystals were prepared by using a hot-injection (thermolysis) method, and all synthesis were carried out under stirring condition and in an inert atmosphere by utilizing a standard air-free technique.

4.3. ZnTe Nanodots and Branched Nanorods. To prepare ZnTe nanodots and branched nanorods, $Zn(Et)_2$ and TOPTe were used as Zn and Te precursor, respectively. TOPTe needs to be prepared freshly by dissolving Te powder into hot TOP (≥250 °C) to form a clear light yellow solution, then $Zn(Et)_2$ was added into this solution after it was cooled to room temperature. To tune the reactivity of $Zn(Et)_2$, TOPO was added into the mixed precursor solution in some cases. Typically, in precursor solution, Zn concentration was in the range of 0.3−0.4 mol/L, while the ratio of Zn/Te (/TOPO) was kept to 1:1 (:0.5). **(i) Spherical ZnTe nanodots:** In a typical reaction, 6 mL of oleylamine or 3 mL of oleylamine plus 3 mL of ODE was added into a 25 mL three-neck flask as stock solvent and was then heated to 270 °C; at that temperature, 1 mL of mixed precursor (Zn + Te) solutions with or without TOPO was swiftly injected into that solution. After injection, the reaction system generally dropped to 260 °C and was kept at that temperature for a specified time (protocol A). **(ii) ZnTe branched nanorods:** 5 g of ODA instead of 6 mL of oleylamine was added into a flask and heated to a specified temperature (220−290 °C); then 1.5 mL of mixed precursor (Zn + Te) solution with or without TOPO was dropped into the system at a rate of 0.3−0.4 mL/min. After precursor addition, the reaction system was kept at that temperature for 5 min (protocol B).

4.4. ZnTe Nanowires. To prepare ZnTe nanowires, a specified amount of zinc oleate (0.4−1.2 mmol) was dissolved in a mixture of 1.5 mL of oleic acid plus 3.5 mL of ODE and heated to 290 °C; then 2 mL of TOPTe (Te powder dissolved in 2 mL of TOP), together with a specified amount of oleylamine, was swiftly injected into this synthetic system. After injection, the system was generally dropped to 250 °C and was kept at that

temperature for 1−3 min (protocol C). To obtain an optimal condition for growth of ZnTe nanowires, various amount of oleylamine (0, 0.5, 1.0, 2 mL) and different Zn/Te ratios (4/1, 2/1, 1/1.5, 1/4) were tested.

4.5. ZnTe Microspheres. A specified amount of zinc oleate (0.2−0.8 mmol) was dissolved in 6 mL of TOA and was heated to 295 °C; then 1.5 mL of TOPTe solution (appropriate amount of Te dissolved in 1.5 mL of TOP to keep Zn/Te ratio as 1:2) was quickly injected, and then the reaction was kept at 280 °C for 3−5 min (protocol D). Continuous and intensive stirring was necessary in above synthesis process.

4.6. ZnTe Hollow Microspheres. As-prepared ZnTe microspheres were purified according to protocol F first and then were redispersed in toluene to form a clear colloidal solution. The colloidal solution was then sonicated in an ultrasonic cleaner for several minutes (protocol E).

4.7. Purification of Nanocrystals. After reaction, the colloid solutions obtained in the above experiments (from protocol A to protocol D) were cooled and precipitated by acetone (or methanol). The formed flocculent precipitate was centrifuged, and the upper layer liquid was decanted; then, the isolated solid was dispersed in chloroform (or toluene). The above centrifugation and isolation procedure was repeated several times for purification of the nanocrystals (protocol F). Finally, the purified nanocrystals were redispersed in chloroform (or toluene) for the preparation of TEM and SEM specimens or dried under vacuum for XRD, XPS, and FTIR characterization.

4.8. Assembly of ZnTe Microspheres. After purification, a colloidal solution of ZnTe microspheres was diluted to specified concentrations. Typically, to prepared 2D and 3D arrays, a colloidal solution containing 1−2% or 4−5% (wt) microspheres was adopted, respectively. Then drops of those colloidal solutions were added on small precleaned Si sheets, and those sheets were then placed in a humid box, which was saturated with toluene vapor, to allow them slow dryness (≥1 h) (protocol G).

4.9. Characterization of ZnTe Nanocrystals. For measurement of the absorption and PL spectra of ZnTe nanocrystals, needle-tip aliquots were taken from reaction flask at given time intervals and dissolved in chloroform. UV−vis absorption spectra were recorded on a Hitachi U-3010 spectrophotometer, while PL spectra were measured on a Hitachi U-4500 spectrophotometer. Infrared spectra were recorded on a PE2000 FTIR with 4 cm^{-1} resolution. To measure the remaining zinc concentration in a synthetic system, inductively coupled plasma atomic emission (ICP) was employed to analyze the aliquots taken from the reaction flask at a given moment; the aliquots must suffer from a standard HCl/HNO_3 digestion before ICP measurements. Scanning electron microcopy (SEM) characterization was done by using a HITACHI S-4800 scanning electron microscope with an X-ray Energy Disperse Spectroscopy (EDS). Transmission electron microscopy (TEM) observations were performed with a JEOL JEM-1011 transmission electron microscope, accompanied by a selected area electron diffraction (SAED). High-resolution transmission electron microscopy (HRTEM) measurements were carried out using a JEOL JEM-2100F transmission electron microscope operated at 200 kV. The specimens for TEM observation were prepared by depositing a drop of a dilute toluene solution of these samples on a carbon-coated copper grid and drying at room temperature. The SEM specimens were prepared by adding drops of dilute solution of ZnTe microspheres on Si substrates according to protocol G. X-ray diffraction (XRD) patterns were recorded by a Rigaku D/max-2400 diffractometer operated at 40 kV voltage and a 200 mA current with Cu K-α1 radiation. XPS data were obtained on a VG-Scientific ESCA Lab 220i-XL spectrometer equipped with a hemisphere analyzer and using Al Kα X-ray as excitation source. Samples for XRD and XPS measurements were solid powder prepared by drying the purified product under vacuum.

4.10. Electrochemical Measurements. Cyclic voltammograms (CVs) were recorded on a Zahner IM6e electrochemical workstation, using glassy carbon discs as the working electrode (~0.25 cm^2), a Pt wire as the counter electrode, a homemade electrode (Ag|0.01 M $AgNO_3$ (in acetonitrile)) as the reference electrode and tetrabutylammoniumhexafluorophosphate ($TBAPF_6$) dissolved in acetonitrile (0.1M) as supporting electrolyte, respectively. All nanocrystals were purified in an inert atmosphere and transferred into a glovebox; therein, these purified nanocrystals were dissolved in chloroform. Drops of these nanocrystal solutions were placed on the surface of working electrodes to form nanocrystal films thereon. The working electrodes were polished, cleaned and dried before depositing the nanocrystal samples. The scan rate was set at 30 mV/s, and the electrolyte solutions were thoroughly deoxygenated by bubbling with high purity nitrogen for 15 min before measurement and a nitrogen atmosphere was maintained over the solutions.

Acknowledgment. This work was supported by the Beijing National Laboratory for Molecular Sciences (BNLMS) of China and the Scientific Research Foundation of Beijing Normal University.

Supporting Information Available: Absorption spectra and TEM images of ZnTe nanodots, ICP result regarding the remaining zinc concentration in synthetic systems, TEM images, HRTEM images, XPS spectra, and FTIR spectra of ZnTe nanowires and microspheres, and CV curves of ZnTe nanocrystals. This material is available free of charge via the Internet at http://pubs.acs.org.